Effect of Corrugated Flute Shape on Fibreboard Edgewise Crush Strength and Bending Stiffness

T.J. URBANIK

The influence of corrugated fibreboard fluting geometry on strength and stiffness is modelled and a method to optimize flute profile is presented. The fluted medium in a corrugated fibreboard is modelled as a connection of curved arc and straight flank segments. Flute pitch, flute height, flank length, arc radius and angle of wrap are normalized to form a set of non-dimensional parameters, two of which can be chosen as independent. Strength and stiffness data from fibreboard with representative flute profiles are used to predict average stress-strain properties of the containerboard components. The strength and stiffness models are then extrapolated to predict theoretically how mechanical properties and material savings change for other flute profiles. The results quantify how an optimum flute profile balances cost, runnability, strength and stiffness.

L'influence de la géométrie des cannelures du carton ondulé sur la résistance et la rigidité est modélisée et une méthode visant à optimiser le profil des cannelures est présentée. La partie cannelée d'un carton ondulé est modélisée comme la connexion d'un arc courbe et de segments latéraux droits. L'écartement des cannelures, la hauteur des cannelures, la longueur latérale, le rayon de l'arc, et l'angle d'enroulement sont normalés pour former un ensemble de paramètres non dimensionnels, dont deux sont sélectionnés comme étant indépendants. Les données sur la résistance et la rigidité du carton avec des profils représentatifs des cannelures sont employées pour prédire les propriétés de contrainte et de déformation des éléments du carton-caisse. Les modèles de résistance et de rigidité sont alors extrapolés afin de prédire de façon théorique les changements en matière de propriétés mécaniques et d'économies matérielles pour d'autres profils de cannelures. Les résultats quantifient la façon dont un profil de cannelure optimal équilibre les coûts, le comportement sur la machine, la résistance et la rigidité.

INTRODUCTION

Corrugated fibreboard has been used as a packaging material for at least 100 years, as evidenced by a history on the evolution of corrugating machines [1]. In the earliest applications, the wave shape (now called A-flute) of the fluted medium imparted thick and soft cushioning, which enabled corrugated fibreboard to compete primarily with straw in packaging for fragile glass. Later, the denser B-flute provided a better printing surface and was more economical than A-flute per unit area of board. The development of the C-flute, which is intermediate in size between A-flute and B-flute, offered a compromise between performance and appearance.

Applications for these commonly used flute profiles have been cited in Item 222 of the motor freight classification system for corrugated fibreboard containers since its inception in 1936 by the National Motor Freight Traffic Association (NMFTA) of the American Trucking Association. However, in response to new practices in the containerboard industry, the NMFTA has de-emphasized attention to flute sizes. As of 1996, Item 222 no longer makes any references to flute profiles. In a cursory investigation, the Fibre Box Association found that one particular corrugating machine manufacturer has been producing around 50 different profiles called C-flute. Performance requirements of corrugated fibreboard that reflect updated distribution and handling practices are now compelling the design of custom profiles to match the weight combinations of linerboard and corrugated medium available through the converter.

One important performance requirement is container stacking strength, which is a function of the edgewise compression strength and bending stiffness of corrugated fibreboard. The objective of this report is to examine theoretically how fluting geometry affects fibreboard strength and stiffness. This paper augments our previous research that examined the effect of containerboard thickness and stress-strain properties on fibreboard strength and stiffness for a fixed flute geometry.

In previous research, we first derived a buckling theory of thin plate structures, appropriate to corrugated fibreboard, and set forth a rationale for distributing fibre between the linerboard and medium components to obtain edgewise compression strength at a minimum weight [2]. An example analyzed a single A-flute profile with fixed containerboard stress-strain properties. Subsequently, we examined theoretically how changing the containerboard stress-strain properties affects the minimum weight design, again with the flute profile fixed [3]. Then our theory was expanded to a programmable buckling model for general plate structures [4].

In this paper, we further implement the model of [4] and examine the influence of fluted geometry on strength and stiffness. Our scope is limited to fixed containerboard-weight

J P P S

T.J. Urbanik
U.S. Dept. Agriculture
Forest Service
Forest Products Lab.
Madison, WI, USA

(turbanik@fs.fed.us)

grades and to fixed stress-strain properties. The collective principles of this and previous research [2–4] can provide the basis for determining optimum containerboard weight, stress-strain property, and flute shape combinations.

BASIC GEOMETRY

The machined surface geometry of most corrugating rolls can be characterized by a sequence of arc sections connected by straight line tangents. The actual shape fabricated into the corrugated fibreboard is a complicated function of numerous process variables and the elastic interaction between paper components subjected to stretching and frictional forces. Previous researchers have sought to simplify the geometry and have advocated sinusoidal, elliptical and trapezoidal shapes, but such shape functions tend to limit the accuracy in accounting for the true fluted length of the corrugated medium and the resulting cost.

Fortunately, the observed shape of defect-free board is close enough to an arc-and-tangent profile to obviate a messy kinematic analysis, although such an analysis might be important to the equipment developer. The arc-and-tangent geometry proposed here is shown in Fig. 1. Flute pitch P, flute height H and tip radius R dimensions are of the middle plane through the corrugated medium, with top-to-bottom symmetry. The tip radius r and the root radius r' of the corrugating rolls differ by at least the caliper T_m of the corrugated medium. (In our discussions, caliper T is used to designate the surface-to-surface thickness. Later, effective thickness t is introduced to designate an equivalent thickness for dealing with stiffness effects.)

Arc-and-tangent corrugations have been analyzed previously for applications to metal roofing, siding and drainage conduits. At first, moment of inertia calculations were of interest [5], but the calculations as presented depend on the graphical determination of various inputs. Wolford [6] generalized the analysis and offered a set of closed form equations. Lou et al. [7] compared the arc-and-tangent 'geometry with sinusoidal and semi-elliptical models and added the fibreboard facings to derive a more general plate bending theory.

Our geometry as shown in Fig. 1 yields a set of equations with more general input parameters than those given in Wolford [6]. and it is more applicable to corrugated fibreboard. Similarity between the two triangles in Fig. 1 establishes the relationships

$$\frac{L}{R} = \frac{H - 2R(1 - \cos\beta)}{R\sin\beta} = \frac{P/2 - 2R\,\sin\,\beta}{R\cos\beta} \quad (1)$$

where L is the length of the flank component in the model. The characterization is more readily obtained in terms of R instead of r and r'. The angle of wrap q is related to the half-angle $\beta = q/2$, as shown. The take-up factor TF, defined as the ratio of the length of the unfluted corrugated medium to the length of the fluted geometry, is given by
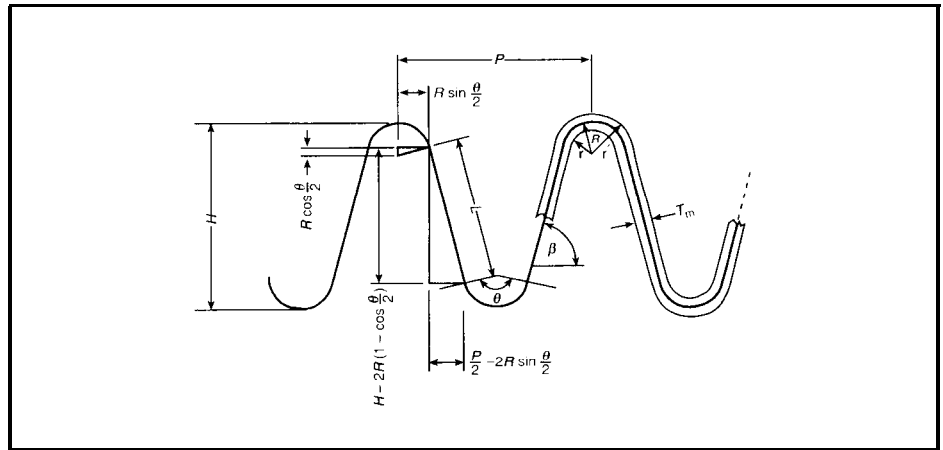

Fig. 1. Arc-and-tangent model through middle plane of corrugated medium.

TABLE I RELATIONSHIPS AMONG NON-DIMENSIONAL PARAMETERS WHEN P, H AND R ARE KNOWN	
Parameter	**Equivalent expression**
β	$\tan^{-1}\left(\dfrac{P/R}{\sqrt{4(H/R)^2 - 16(H/R) + (P/R)^2}}\right) + \tan^{-1}\left(\dfrac{2(H/R)-4}{P/R}\right)$
TF	$\dfrac{P/R - 4\sin\beta}{(P/R)\cos\beta} + \dfrac{4\beta}{P/R}$
	$\dfrac{2\cos\beta + 2\beta\sin\beta + H/R - 2}{(H/R - 2)\cos\beta + 2}$
	$\dfrac{(2\beta H/P - 1)\cos\beta - (\beta + 2H/P)\sin\beta + 1}{\cos\beta - 1}$

TABLE II RELATIONSHIPS AMONG NON-DIMENSIONAL PARAMETERS WHEN P, H AND TF ARE KNOWN	
Parameter	**Equivalent expression**
β	$\sin^{-1}\left(\dfrac{(2\beta(H/P) - TF - 1)\cos\beta + TF + 1}{\beta + 2(H/P)}\right)$
$\dfrac{P}{R}$	$\dfrac{4(\beta - \tan\beta)}{TF - \sec\beta}$
$\dfrac{H}{R}$	$\dfrac{H}{P}\dfrac{P}{R}$

$$TF = \frac{2L + 2Rq}{P} \quad (2)$$

There is a benefit to expressing the basic geometry in terms of the non-dimensional parameters P/R, H/R, H/P TF and β, in that, given any two of these parameters, the remaining three are determinable from Eqs. (1) and (2). A set of relationships among these parameters is given in Tables I and II. If P, H and R are known from the corrugating rolls, Table I can be used to determine β in terms of H/R and P/R, followed by the solution for TF in terms of β and either P/R, H/R or H/P. Sometimes R is unknown, but P, H and TF can be determined from the combined corrugated fibreboard. For this case, Table II gives solutions for β in terms of H/P, TF and an estimated β, for P/R in terms of β and TF and for H/R in terms of H/P and P/R.

Note that β in Table II needs to be computed with successive iterations. Thus, an initial estimate, i.e. $\beta = 1$, yields an improved estimate, etc. until convergence.

In examining graphically the relationships among the various non-dimensional parameters, TF and q were chosen as the independent variables. Figure 2 shows contours of constant levels of H/P and P/R corresponding to variations in TF and q Figure 2 was produced from the relationships given in Tables I and II over a range of interest typical of conventional corrugated fibreboard profiles. At a point (off the graph) where $P/R = 4$, $H/P = 0.5$ and $q = 180°$, the geometry would consist of a connection of semicircular arcs without connecting flanks. As R approaches 0, P/R approaches infinity and the geometry in the upper left corner
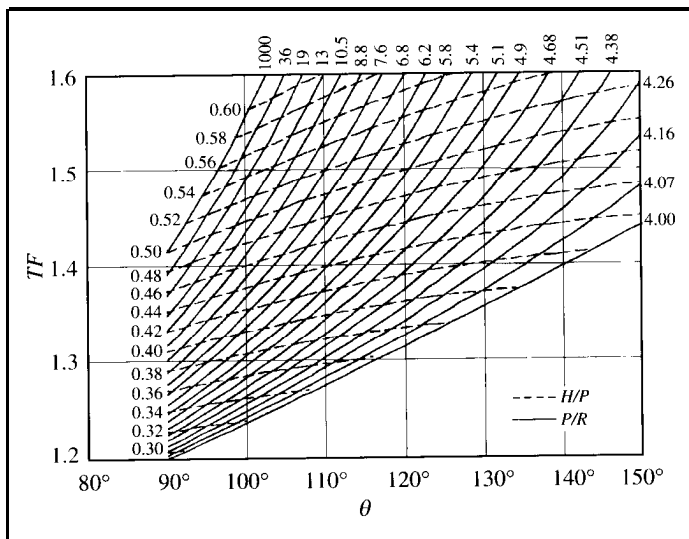
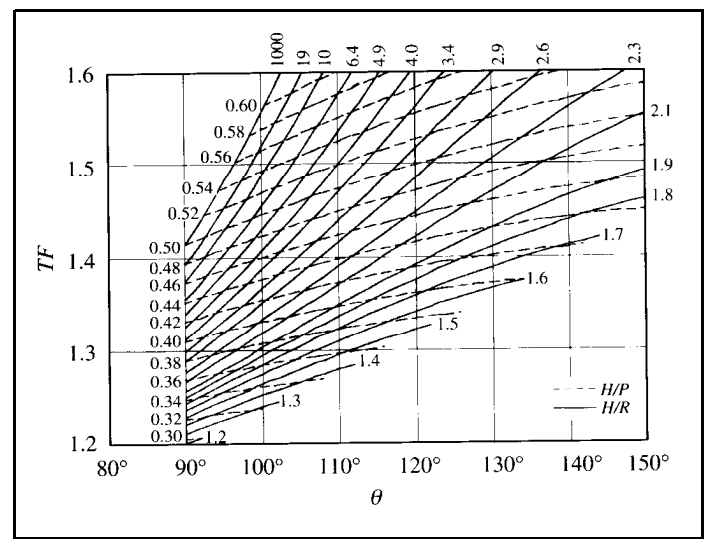**Fig. 2. Contours of constant levels of *H/P* and *P/R* corresponding to *TF* and *q* in arc-and-tangent model.**

Fig. 3. Contours of constant levels of *H/P* and *H/R* corresponding to *TF* and *q* in arc-and-tangent model.

			TABLE III				
			TYPICAL FLUTE PROFILES				
Flute	**P** (mm)	**H** (mm)	**TF**	**H/P**	**P/R**	**H/R**	**q** (°)
A	8.47	4.57	1.56	0.540	5.78	3.12	123
C	7.21	3.46	1.48	0.480	4.92	2.36	124
B	6.35	2.54	1.36	0.400	4.33	1.73	119

of Fig. 2 approaches an increasingly large triangular shape without arcs. Figure 2 readily shows what geometry must change to reduce *TF,* in order to reduce the amount and cost of corrugated medium for instance. Figure 3 shows contours of constant levels of *H/R.*

Typical flute profiles are given in Table III. These profiles were obtained by fitting our arc-and-tangent model to the caliper T_b data on combined corrugated fibreboard in McKee et al. [8] in combinations of four material grades and three flute sizes. A more complete discussion of this is given in the Appendix. In the analyses of choosing an optimum profile, as presented in the following sections of this report, the C-flute profile in Table III was used as a standard or reference profile.

RUNNABILITY

Before any flute profile can be considered, the corrugator must be able to run. Hoke and Gottsching [9] examined the effect of fluting geometry on the frequency of mechanical fractures occurring in the medium during corrugation. They found that increasing *q* increases the frictional forces during corrugation and causes a higher frequency of fractures to occur in the flute flank. These researchers also found that reducing *r* increases the bending stress around the flute tip in the medium and leads to more flute breaks at that point.

Predictions based on these data [9] and applied to our standard profile are given in Fig. 4, which shows the frequency of corrugation breaks, relative to the frequency of breaks at the reference profile, for eight flute profiles. The standard profile lies at the intersection of contour *H/P* = 0.48 and contour *P/R* = 4.92. Along the contour *H/P* = 0.48, *H* and *P* were fixed while *R* varied among four profiles, as indicated by the corresponding four points. Along the contour *P/R* = 4.92, *P* and *R* were fixed while *H* varied. Lastly, along the contour *H/R* = 2.36, *H* and *R* were fixed while *P* varied.

It can be inferred from Fig. 4 that geometry obtained by either reducing *H* or increasing *P,* while fixing *R,* reduces *TF* and the associated

cost and also favourably reduces the frequency of corrugation breaks. In contrast, reducing *R,* while fixing *P* and *H,* to obtain a lower *TF* adversely increases the frequency of breaks.

EDGE CRUSH STRENGTH

The stress-strain properties of the linerboard and corrugated medium components constituting 10 flute and grade combinations of corrugated fibreboard were predicted as described in the Appendix. Comparisons between average experimental edgewise crush test (ECT) strength and the strength predictions based on those properties are given in Table V in the Appendix. The nominal 205 g/m² (42 lb/ 1000 ft²) facings, a nominal 127 g/m² (26 lb/1000 ft²) corrugated medium and their respective stress-strain properties representing the 1.38 MPa (200 lb) series of corrugated fibreboard components were considered as standard or reference paper properties and ECT strength was calculated for various fluting geometry using the model in [4]. (Note: In this paper, pound units rather than pounds per square inch are used for bursting strength to be consistent with the original McKee et al. [8] data.)

The ECT strength of our standard profile composed of our standard components was predicted to be 8.15 kN/m (Table V). Figure 5 shows contours of constant levels of ECT strength, normalized with respect to ECT strength at the standard profile, for other *TF* and *q* combinations. The material properties and paper basis weights remain fixed for all profiles. For instance, at coordinates *TF* = 1.48 and *q* = 124°, i.e. our C-flute profile standard, Fig. 5 shows that ECT strength differs by 0% from the

standard condition, an obvious result. For the A-flute profile with *TF* = 1.56 and *q* = 123° (Table III), Fig. 5 shows that ECT strength differs by -4.9% from the standard condition. This is the same result obtained if the predicted ECT strength of 7.75 kN/m for the 200 lb A-flute fibreboard in Table IV is compared directly with the 8.15 kN/m ECT strength at the standard profile (Table V).

This interesting example shows a case where ECT strength actually decreases with the addition of material in switching from C-flute to A-flute. The mechanism of failure by local buckling that explains this result was the subject of a previous research study [2]. In a later study [3], we showed how increasing the initial modulus of elasticity of a containerboard component can, under certain conditions, also reduce ECT strength.

Figure 5 was produced with *R* = 1.52 mm, but it can be applied to other scales of geometry proportional to *P, H* and *R* provided that the same material stress-strain properties prevail. To this end, contours of constant levels of *H/P* are superimposed in Fig. 5. Note that the ECT strength of profiles in the upper left corner of Fig. 5 diminishes to zero (i.e. 100% strength reduction from standard condition) because, as *P* and *H* approach infinity at those profiles, with *R* fixed, the local buckling strength of the corrugated fibreboard structure approaches zero.

BENDING STIFFNESS

Bending stiffness *El* data on the 10 flute and grade combinations of corrugated fibreboard are given in Table V of the Appendix. For a narrow corrugated fibreboard beam, the model we use for *EI* is the sum of linerboard
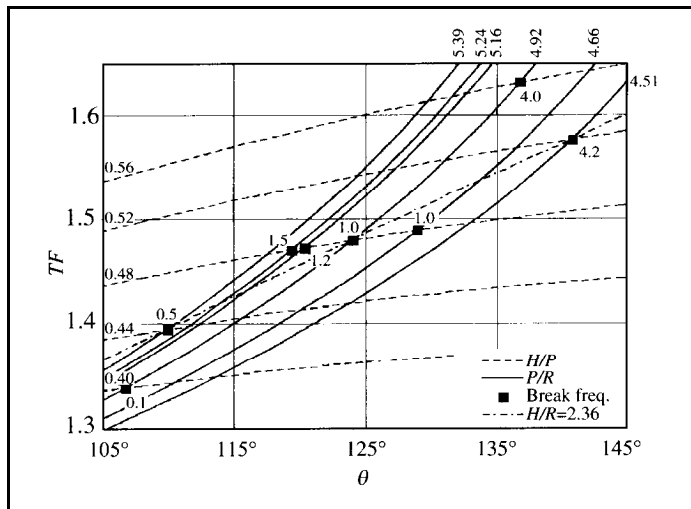
Fig. 4. Frequency of fractures occurring in corrugated medium relative to frequency of fractures observed for a standard profile, for eight flute profiles. Contours of constant levels of *H/P, P/R* and *H/R* specify the profile geometry. Points correspond to eight specific profiles and numbers correspond to their relative fracture frequencies.
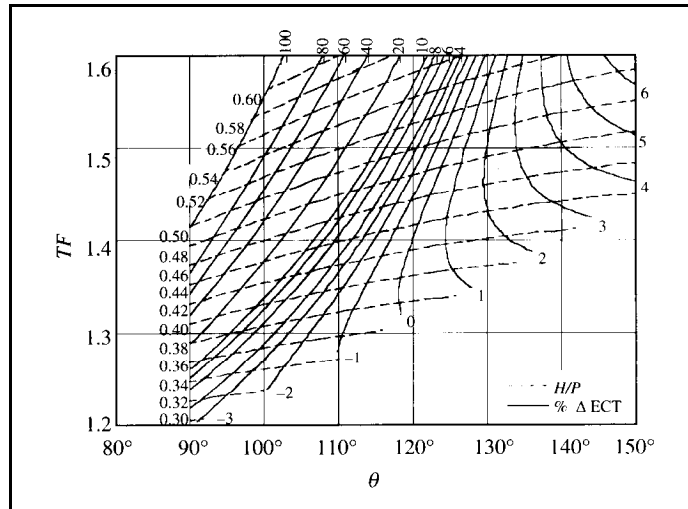

Fig. 5. Contours of constant levels of ECT strength (expressed as percentage of difference from standard profile) and contours of constant levels of *H/P*. Linerboard and corrugated medium stress–strain properties are fixed at standard conditions and *R* = 1.52 mm in all ECT calculations.

and corrugated medium *EI* components in the direction of bending as given by

$$El = E_l I_l + E_m I_m \qquad (3)$$

where E_l and E_m are initial moduli of elasticity in the direction of strain of linerboard and medium material, respectively, and I_l and I_m are moment of inertia expressions for the combined linerboard facings and the corrugated medium, respectively. Expressions for determining I_l and I_m are given in Table IV where they are normalized with respect to the combined board *P* and to either the linerboard caliper T_l or the medium caliper T_m. The expression for I_m is further divided into expressions I_f and I_t for the flute flank and tip components, respectively. For brevity we have omitted the derivation of these expressions, obtainable from [7], and have simply manipulated the expressions into a form with non-dimensional inputs.

As written, Eq. (3) is applicable when bending occurs in the cross-machine direction (CD), i.e. when the flutes are aligned with the length of the beam. The I_m components in Table IV are relevant to this case only. With machine-direction (MD) bending, the stiffness contributed by the corrugated medium is negligible and the second term in Eq. (3) can thus be ignored. Calculations of *EI* for the combined boards represented in Table V revealed that the

corrugated medium contributes around 6–13% to the total combined board stiffness, depending on the flute profile and grade.

The predicted *El* levels in Table V were determined for MD and CD bending from the moment of inertia effects contributed by only the facings, i.e. $EI = E_l I_l$, which enabled us to estimate the extensional stiffness of the facing material. Details on this estimation process are given in the Appendix. The *EI* of corrugated

fibreboard with our standard profile and standard materials is predicted to be 14.04 Nm for MD bending and 5.92 Nm for CD bending (Table V). The geometric mean stiffness $EI_{gm} = 9.12$ Nm. If the corrugated medium is included, the more accurate $EI_{gm} = 10.2$ Nm.

Figure 6 shows contours of constant levels of EI_{gm}, normalized with respect to the EI_{gm}, at the standard profile, for other *TF* and q combinations. Calculations are based on Eq. (3). As

TABLE IV
NON-DIMENSIONAL MOMENT OF INERTIA COMPONENTS

Term	Equivalent expression
$\dfrac{I_l}{PT_l^3}$	$\dfrac{1}{2}\left(\dfrac{T_b}{T_l} - 1\right)^2 + \dfrac{1}{6}$
$\dfrac{I_t}{PT_m^3}$	$\dfrac{R}{P}\left(\left(4\left(\dfrac{R}{T_m}\right)^2 + 1\right)\dfrac{\sin\theta + \theta}{4} + \left(12\left(\dfrac{R}{T_m}\right)^2 + 1\right)\left(\dfrac{H}{R} - 2\right)\dfrac{\sin\beta}{3} + \left(\dfrac{R}{T_m}\right)^2\left(\dfrac{H}{R} - 2\right)^2\beta\right)$
X	$\dfrac{R}{T_m}\left(\dfrac{1}{2}\dfrac{P}{R}TF - \theta\right)$
$\dfrac{I_f}{PT_m^3}$	$\dfrac{1}{6}\dfrac{T_m}{P}\left(x^3\sin^2\beta + x\cos^2\beta\right)$
$\dfrac{I_m}{PT_m^3}$	$\dfrac{I_t}{PT_m^3} + \dfrac{I_f}{PT_m^3}$

TABLE V
MECHANICAL PROPERTIES OF COMBINED CORRUGATED FIBREBOARD

| Flute	Series	BW	T_b			E/MD			E/CD			ECT		
	(lb)	(g/m²)	exp. (mm)	pred. (mm)	diff. (%)	exp. (Nm)	pred. (Nm)	diff. (%)	exp. (Nm)	pred. (Nm)	diff. (%)	exp. (kN/m)	pred. (kN/m)	diff. (%)
A	175	366	5.13	5.18	0.9	21.24	20.76	−2.3	9.08	9.09	0.0	7.29	7.06	−3.1
	200	410	5.23	5.22	−0.2	22.71	23.15	1.9	9.72	9.76	0.5	7.92	7.75	−2.0
	275	674	5.54	5.50	−0.7	28.81	30.51	5.9	15.93	16.13	1.3	10.53	11.09	5.3
C	175	366	4.14	4.07	−1.7	12.43	12.56	1.0	5.54	5.50	−0.7	7.43	7.53	1.4
	200	410	4.06	4.11	1.2	14.91	14.04	−5.9	6.09	5.92	−2.8	7.72	8.15	5.6
	275	674	4.52	4.39	−3.0	20.56	18.80	−8.6	10.06	9.94	−1.2	11.03	11.28	2.2
	350	879	4.45	4.60	3.5	23.50	23.50	0.0	8.65	8.65	0.0	13.27	12.77	−3.8
B	175	366	3.02	3.15	4.1	6.15	7.30	18.8	3.13	3.20	2.1	7.60	7.59	−0.2
	200	410	3.15	3.19	1.4	7.93	8.19	3.3	3.30	3.46	4.7	8.27	8.16	−1.3
	275	674	3.63	3.46	−4.6	12.88	11.21	−13.0	6.27	5.93	−5.5	11.42	11.14	−2.5
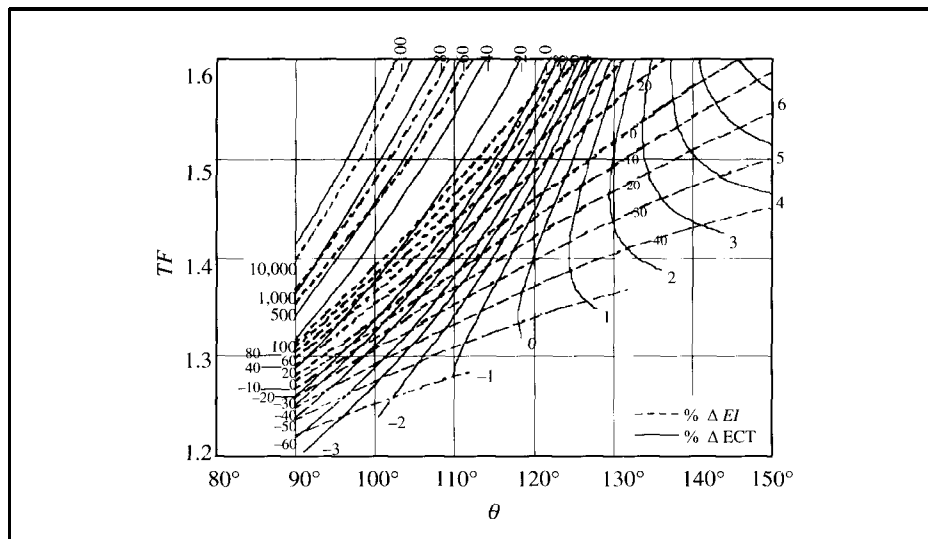
Fig. 6. Contours of constant levels of ECT strength and EI_{gm} (expressed as percentage of difference from standard profile). Linerboard and corrugated medium stress-strain properties are fixed at standard conditions and $R = 1.52$ mm in all calculations.

Fig. 7. Variation of average caliper T_b of combined corrugated fibreboard with minimum combined facing basis weight required at time of study. Points are average T_b levels for three flute sizes [8] and lines are regression parallels.

in the case of the ECT calculations, the material properties and paper basis weights remain fixed for all profiles. For the A-flute profile with $TF = 1.56$ and $q = 123°$ (Table II), for example, Fig. 6 shows that EI_{gm} differs by 66% from the standard condition. To enable Fig. 6 to be used to determine the strength and stiffness benefits in changing the flute profile, contours of constant levels of ECT strength are superimposed.

CONCLUSION

In this study, an arc-and-tangent model was used to represent the geometry of the fluted medium in a corrugated fibreboard structure. Formulas for translating corrugating roll geometry into dimensional inputs to a plate structure model are given. We provide a method for fitting models of fibreboard edgewise compression strength and bending stiffness to mechanical property data on the combined board and predicting average stress-strain properties of the components. Then, using a standard set of papers as inputs: these models were extrapolated to examine theoretically how performance and material savings are predicted to change for other arbitrary flute profiles. The
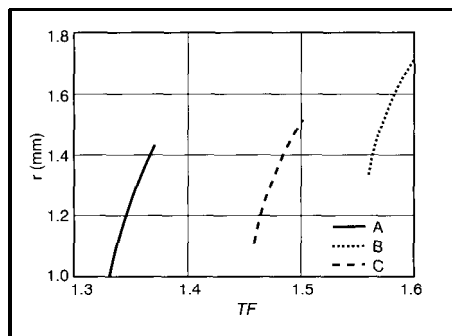
results quantify how an optimum flute profile balances cost, runnability, strength and stiffness. Combining these results with previous research on fibre distribution and stress-strain properties can provide the basis for determining optimum containerboard weight, stress-strain property and flute shape combinations.

APPENDIX

In the study by McKee et al. [8], nine companies supplied corrugated fibreboard material in combinations of three flute sizes and four weight grades (series). The averages of the combined board caliper T_b, EI and ECT strength data for each flute and series combination are reported in Table V. The basis weights BW correspond to the minimum carrier requirements for the combined weight of facings, as were in effect at the time of the study.

The variation of T_b with BW (Fig. 7) leads to predictions of H for each flute. From the y-axis intercepts we obtain, assuming parallel regression lines, $H + T_m = 4.81$, 3.69 and 2.70 mm for A-, C- and B-flute, respectively,
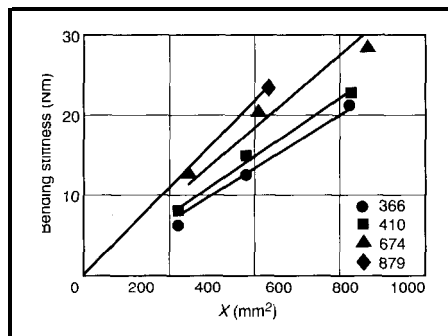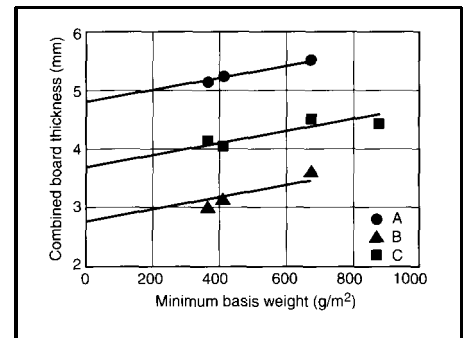
and if the minimum carrier requirement for the corrugated medium that $T_m = 0.229$ mm is applied, these intercepts predict respective flute heights (H) of 4.57, 3.46 and 2.54 mm.

Take-up factors for the A-, C- and B-flutes, representing the industry in general, were reported to be 1.56, 1.42 and 1.36, respectively [8]. The plots in Fig. 8 show how r varies with TF if the previous levels of H and T_m are held fixed. Implicitly, the plots yield H/R and thus P/R. If we represent all the flute profiles with a single $r = 1.41$ mm, which is consistent with the magnitudes reported in Down [10], our model predicts levels of $P = 8.47$, 7.21 and 6.35 mm for A-, C- and B-flutes, respectively, which are within the industry's specified tolerances [11]. Flute geometry is summarized in Table III.

Given the EI and the extensional stiffness Et of a laminate, an effective thickness $t = \sqrt{12\, EI\, /\, Et}$ yields the same modulus of elasticity E for both bending and extension. In general $t < Tf$ for paper. Substituting the expression for I_l of combined board (Table IV) into EI of combined board and rearranging the terms lead to the formula

$$EI \approx E_l t_l \left[\frac{(T_b - T_l)^2}{2} + \frac{T_l^2}{6} \right] = E_l t_l X \qquad (4)$$

Fig. 8. Variation of radius of curvature r of flute tip with combined board take-up factor TF when flute height $H = 4.57$, 3.46 and 2.54 mm, corresponding to A-, C- and B-flute profiles, respectively, and corrugated medium caliper $T_m = 0.229$ mm.

Fig. 9. Variation of bending stiffness of combined corrugated fibreboard in machine direction (MD) with parameter X from Eq. (4). Points are data from 3 flute sizes and 4 combined basis weights (BW) of facing material in grams per square metre. Lines are regressions through the origin. Slope of each line through data for each BW is linerboard extensional stiffness in MD.
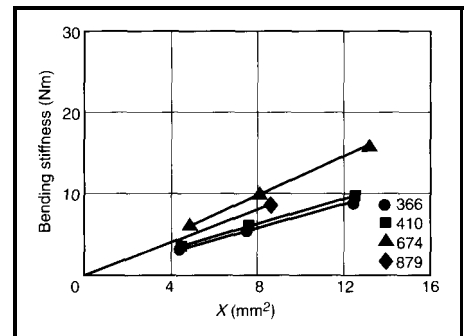

Fig. 10. Variation of bending stiffness of combined corrugated fibreboard in cross-machine direction (CD) with parameter X from Eq. (4). Points are data from 3 flute sizes and 4 combined basis weights (BW) of facing material in grams per square metre. Lines are regressions through the origin. Slope of each line through data for each BW is linerboard extensional stiffness in CD.

Flute	Series (lb)	T_b (mm)	$H+T_m$ (mm)	T_1 (mm)	X (mm^2)	E_1t_1 (kN/m) MD	CD
A	175	5.18	4.80	0.189	12.45	1667	729
	200	5.22	4.80	0.212	12.57	1842	777
	275	5.50	4.80	0.348	13.27	2299	1215
C	175	4.07	3.69	0.189	7.53	1667	729
	200	4.11	3.69	0.212	7.62	1842	777
	275	4.39	3.69	0.348	8.18	2299	1215
	350	4.60	3.69	0.454	8.62	2725	1003
B	175	3.15	2.77	0.189	4.38	1667	729
	200	3.19	2.77	0.212	4.45	1842	777
	275	3.46	2.77	0.348	4.88	2299	1215

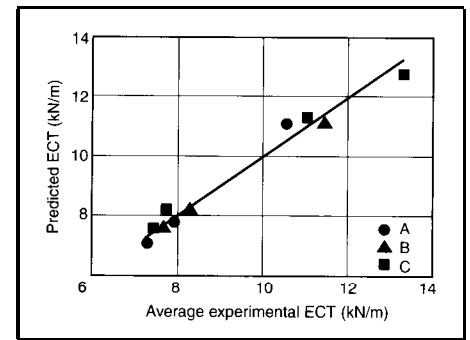**TABLE VI — DETERMINATION OF FACING EXTENSIONAL STIFFNESS**

Fig. 11. Comparison between ECT strength predictions, based on optimum set of containerboard stress-strain properties and data for 3 flute sizes.

TABLE VII — ECT PLATE ELEMENT PROPERTIES

Flute	Series (lb)	Facing t (mm)	l (mm)	(MPa)	(GPa)	A	Medium t (mm)	l (mm)	c_1 MPa	c_2 (Gpa)	A
A	175	0.241	8.47	10.1	3.02	2.28	0.229	6.61	10.1	2.90	2.24
	200	0.264	8.47	10.1	2.94	2.37	0.229	6.61	10.1	2.90	2.24
	275	0.400	8.47	10.1	3.03	1.89	0.229	6.61	10.1	2.90	2.24
C	175	0.241	7.21	10.1	3.02	2.28	0.229	5.33	10.1	2.90	2.24
	200	0.264	7.21	10.1	2.94	2.37	0.229	5.33	10.1	2.90	2.24
	275	0.400	7.21	10.1	3.03	1.89	0.229	5.33	10.1	2.90	2.24
	350	0.506	7.21	10.1	1.98	2.72	0.229	5.33	10.1	2.90	2.24
B	175	0.241	6.35	10.1	3.02	2.28	0.229	4.32	10.1	2.90	2.24
	200	0.264	6.35	10.1	2.94	2.37	0.229	4.32	10.1	2.90	2.24
	275	0.400	6.35	10.1	3.03	1.89	0.229	4.32	10.1	2.90	2.24

in which X is the expression contained in parentheses. The first term of X accounts for facing extensional energy contributions to EI. The second term accounts for bending energy contributions. The approximation results from substituting T_1 for t_1 in the second term and from neglecting the corrugated medium.

Table VI gives the X levels derived from the T_b and $H + T_m$ predictions. When the combined board $EI - X$ data are plotted as shown in Figs. 9 and 10, it is readily established by Eq. (4) that the slope of each regression line through each series of data is the average value of E_1t_1 representing the series in the respective direction of bending. Combined board EI predictions from the regression lines are given in Table V and the predicted facing E_1t_1 levels are given in Table VI.

In the plate structure model of Johnson and Urbanik [4], ECT strength is determinable from t, width l and stress-strain constants in the relationship $\sigma = c_1 \tanh(c_2 / c_1\varepsilon)$ for facing and medium microplate elements as given in Table VII. Facing and medium microplate l dimensions are given by P and $P \cdot TF/2$, respectively. For facing elements, the stress-strain constant c_2 is given by E_1t_1/t_1 in the CD (Table VI) and A is the ratio of MD E_1t_1 to CD E_1t_1. Medium stress-strain properties were taken as the average of facing properties. An optimum value of $c_1 = 10.1$ MPa and optimum thickness functions of $t_1 = T_1 - 0.052$ mm were determined for facing microplates and $t_m = 0.229$ mm for medium microplates. Although numerous scenarios could obviously be found for optimizing the

missing data, the optimization chosen herein was found to yield stress-strain curves and t levels that are consistent with typical paper properties. ECT strength predictions are given in Table V and compared with data in Fig. 11.

REFERENCES

1. MALTENFORT, G.G., "Corrugated Shipping Containers: An Engineering Approach", Jelmar Publishing Co., Inc., Plainview, New York (1988).
2. JOHNSON, M.W., Jr., URBANIK, T.J. and DENNISTON, W.E., "Optimum Fibre Distribution in Singlewall Corrugated Fibreboard", Res. Paper FPL 348, U.S. Dept. Agriculture, Forest Service, Forest Products Laboratory (1979).
3. URBANIK, T.J., "Effect of Paperboard Stress–Strain Characteristics on Strength of Singlewall Corrugated Fibreboard: A Theoretical Approach", Res. Paper. FPL 409, U.S. Dept. Agriculture, Forest Service, Forest Products Laboratory (1981).
4. JOHNSON, M.W., Jr. and URBANIK, T.J., "Analysis of the Localized Buckling in Composite Plate Structures With Application to Determining the Strength of Corrugated Fibreboard", J. Composites Tech. Res. 11(4):121–127 (1989).
5. BLODGETT, H.B., "Moment of Inertia of Corrugated Sheets", Civil Engr. 4(9):492–493 (1934).
6. WOLFORD, D.S., "Sectional Properties of Corrugated Sheets Determined by Formula," Civil Engr. Feb. (59–60):103–104 (1954).
7. LUO, S., SUHLING, J.C., CONSIDINE, J.M. and LAUFENBERG, T.L., "The Bending Stiffness of Corrugated Board", Mechanics of Cellulosic Materials, ASME, AMD–Vol. 145/MD–Vol. 36, 15–26 (1992).
8. McKEE, R.C., GANDER, J.W. and WACHUTA, J.R., "Compression Strength Formula for Corrugated Boxes", Paperboard Packaging 48(8):149–159 (1963).
9. HOKE, U. and GOTTSCHING, L., "Physical Technological Characterization of The Corrugating Process. Part IIIb: Forming of Corrugations as a Function of Profile Geometry— Assumptions and Investigations", Wochbl. Papierfabr. 111(7):207–208, 210–212, 214; (8):251–256, 258 (1983).
10. DOWN, A.G., "The Effect of Flute Profile Changes on Take-Up Ratio and Medium Cost", Proc. Corrugator Rolls Workshop, TAPPI Corrugated Containers Conf. (1983).
11. "Fibre Box Handbook", Fibre Box Association, Chicago, IL, USA (1976).